PRELIMINARY: Relative measurements, lagrangian correlations from a radiosonde cluster dataset

Analysis of dataset from cluster launches during WESCON 2023 (Chilbolton, UK)

Prepared by Shahbozbek Abdunabiev, Daniela Tordella

DISAT, Politecnico di Torino

February 2, 2024

Below, the reader can find a set of figures and tables, distributed in the following sections. At the moment, no text has been included.

1 Experiment context **2**

2 Dispersion of the radiosonde cluster across the experimental domain in the Chilbolton site. First post processing of data concerning probe trajectories, encounters with clouds (averages in time (hourly) and in altitude layers) and stratification level fluctuations... **2**

3 Relative dispersion analysis via distance - neighbor graph (Richardson, 1926) **8**

4 Relative measurements and local turbulent characteristics from cluster dataset **10**

5 Lagrangian correlation analysis **13**

6 From DNS simulation dataset **13**

1 Experiment context

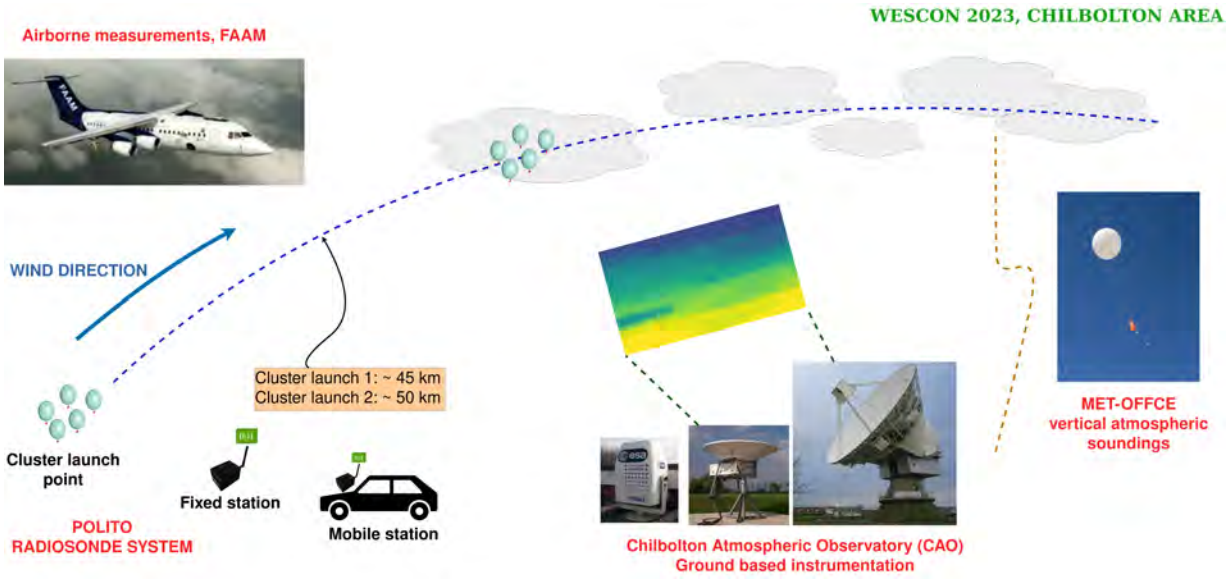

Figure 1: The experimental context for WESCON 2023 involved cluster launches of the POLITO radiosonde system conducted on the intensive observation period (IOP) days, which took place on July 5-6, 2023. Throughout these IOP days, a comprehensive observational dataset was also obtained through the instrumentation of both the UK MET-OFFICE and the Chilbolton Observatory Facility (NCAS).

2 Dispersion of the radiosonde cluster across the experimental domain in the Chilbolton site. First post processing of data concerning probe trajectories, encounters with clouds (averages in time (hourly) and in altitude layers) and stratification level fluctuations...

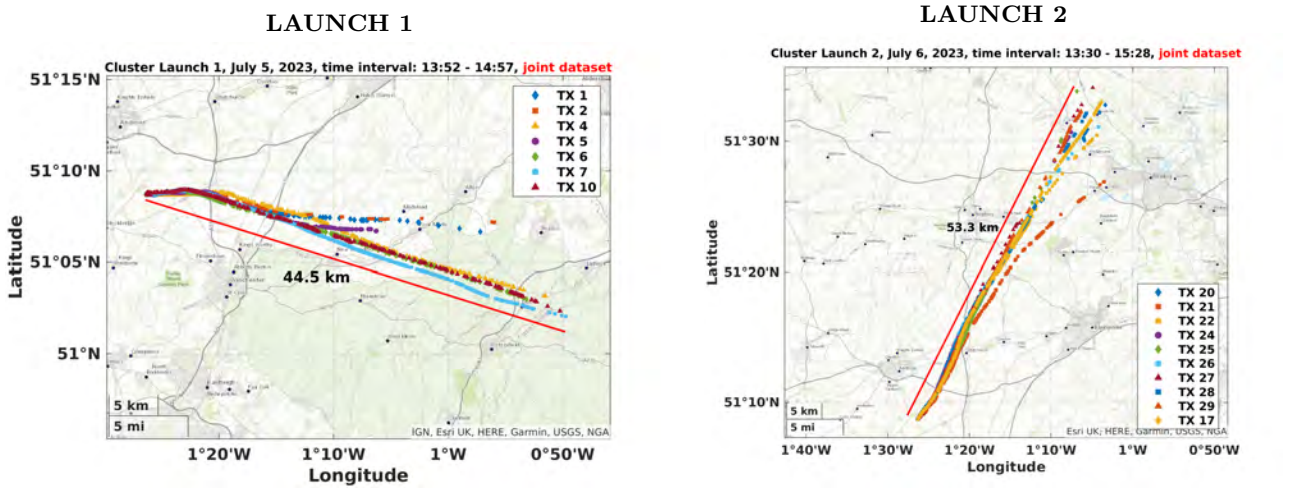

Figure 2: Trajectories of radiosondes during two flights. Data transmission continued during the experiments for about 1.5 hour until the radioprobe reached almost $\sim$ 50 km in horizontal distance. The dispersed cluster of the radiosonde remained within the boundary layer during the flight (500 – 2000 meters). We received packets each 4–5 seconds on average from radiosondes.

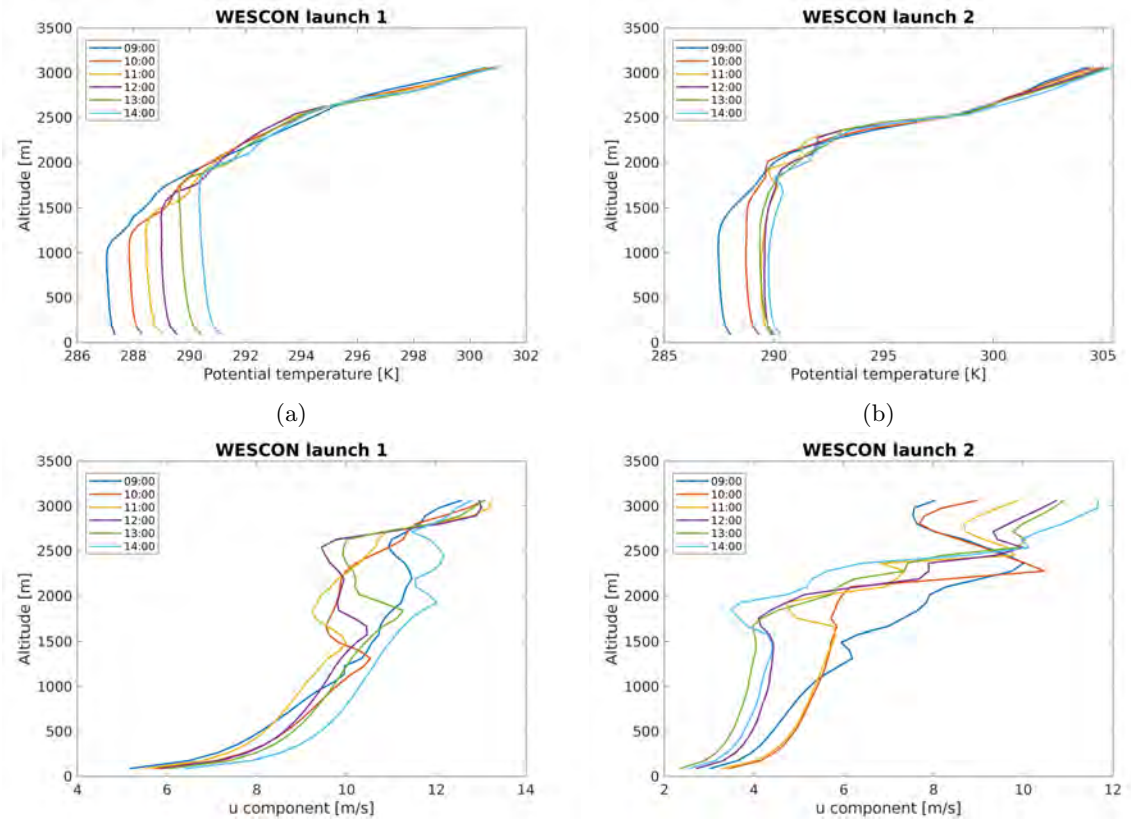

(a)

(b)

(c) Eastward wind component

(d) Eastward wind component

Figure 3: Vertical profiles of potential temperature and eastward wind velocity obtained from CLOUDNET and post-processed. Data correspond to IOP temporal windows matching our in-field launches, WESCON 2023 campaign. Launch 1 was carried out on July 5 and launch 2 on July 6.

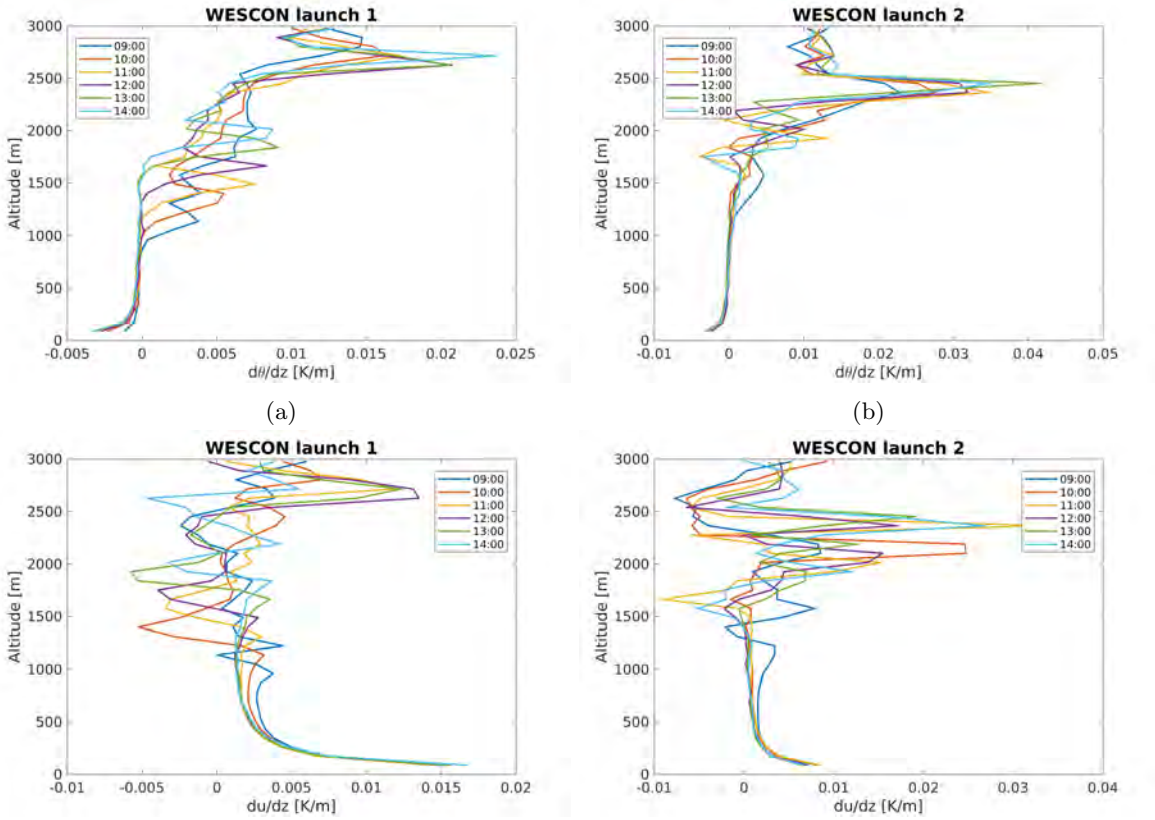

Figure 4: Vertical gradients of potential temperature and eastward wind velocity obtained from CLOUDNET and post-processed. Data correspond to IOP temporal windows matching our in-field launches, WESCON 2023 campaign. Launch 1 was carried out on July 5 and launch 2 on July 6.

Quantity\Day	Day 1 – July 5, 2023 11:00 – 12:00 UTC		Day 2 – July 6, 2023 11:00 – 12:00 UTC	
	[80 – 400 m]	[2500 – 3000 m]	[80 – 400 m]	[2500 – 3000 m]
Potential temperature (θ) [K]	289.0	296.9	289.6	301.3
Eastward Velocity (zonal wind component, u) [m/s]	7.3	11.5	3.8	9.5
Northward Velocity (meridional wind component, v) [m/s]	-1.8	-1.6	5.6	7.7
Horizontal wind, HWS = (u^2+v^2) ^ (0.5)	7.5	11.6	6.8	12.2
∂θ/∂z *[K/m]*	-0.0013	0.0134	-0.001	0.01
∂u/∂z *[1/s]*	0.007	0.007	0.004	0.004
∂HWS/∂z *[1/s]*	0.008	0.007	0.007	0.002
Richardson number, g*(∂θ/∂z)/(∂u/∂z) ^2	-260	2682	-613	6130
Richardson number, g*(∂θ/∂z)/(∂HWS/∂z) ^2	-200	2682	-200	2.4*10^4

Figure 5: CLOUDNET observed potential temperature, zonal wind velocity component and horizontal wind speed during the hours when the infield cluster launches were performed, WESCON campaign, July 5-6 2023. Mean values are reported. Click here to download day 1 data on July 5, 2023. Click here to download day 2 data on July 6, 2023.

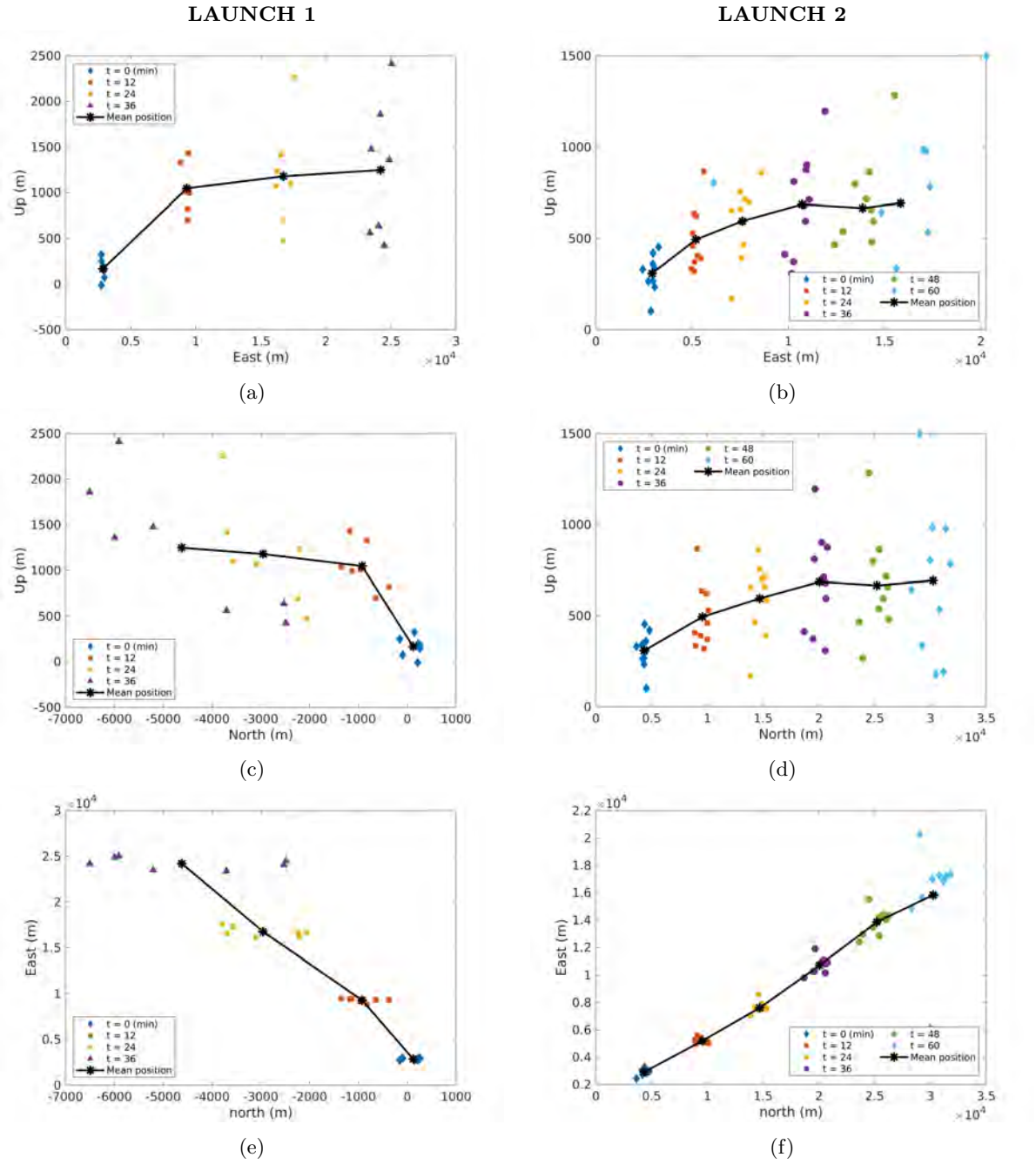

Figure 6: The radiosondes were dispersed along different planes: east-up, north-up, and north-east. The left panels highlight the first launch, while the right panel shows the second launch.

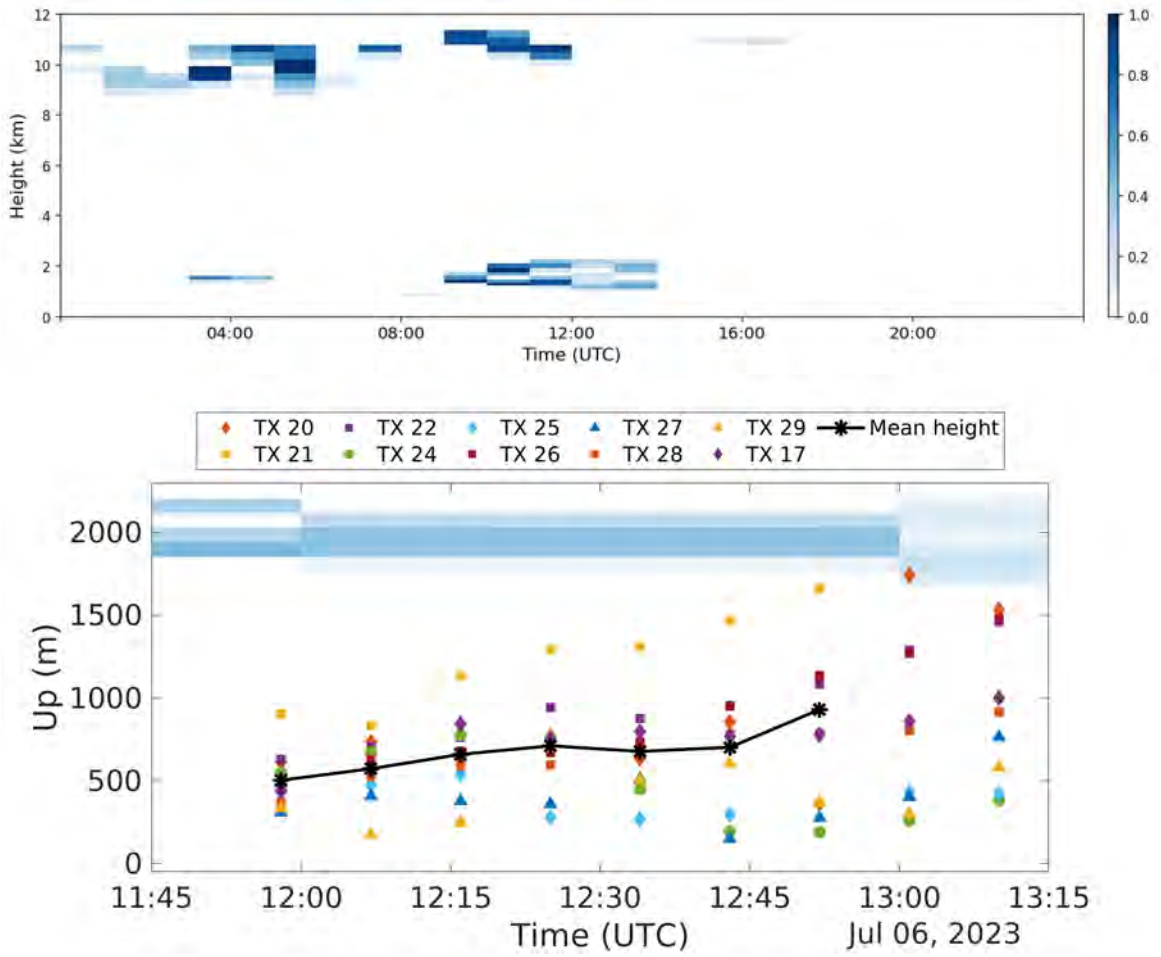

Figure 7: A floating cluster of radiosondes are approaching to the boundary layer clouds. Cloud fraction is generated using ECMWF(European Centre for Medium-Range Weather Forecasts) IFS forecast model using Chilbolton CL51 ceilometer and/or Chilbolton Copernicus cloud radar dataset.

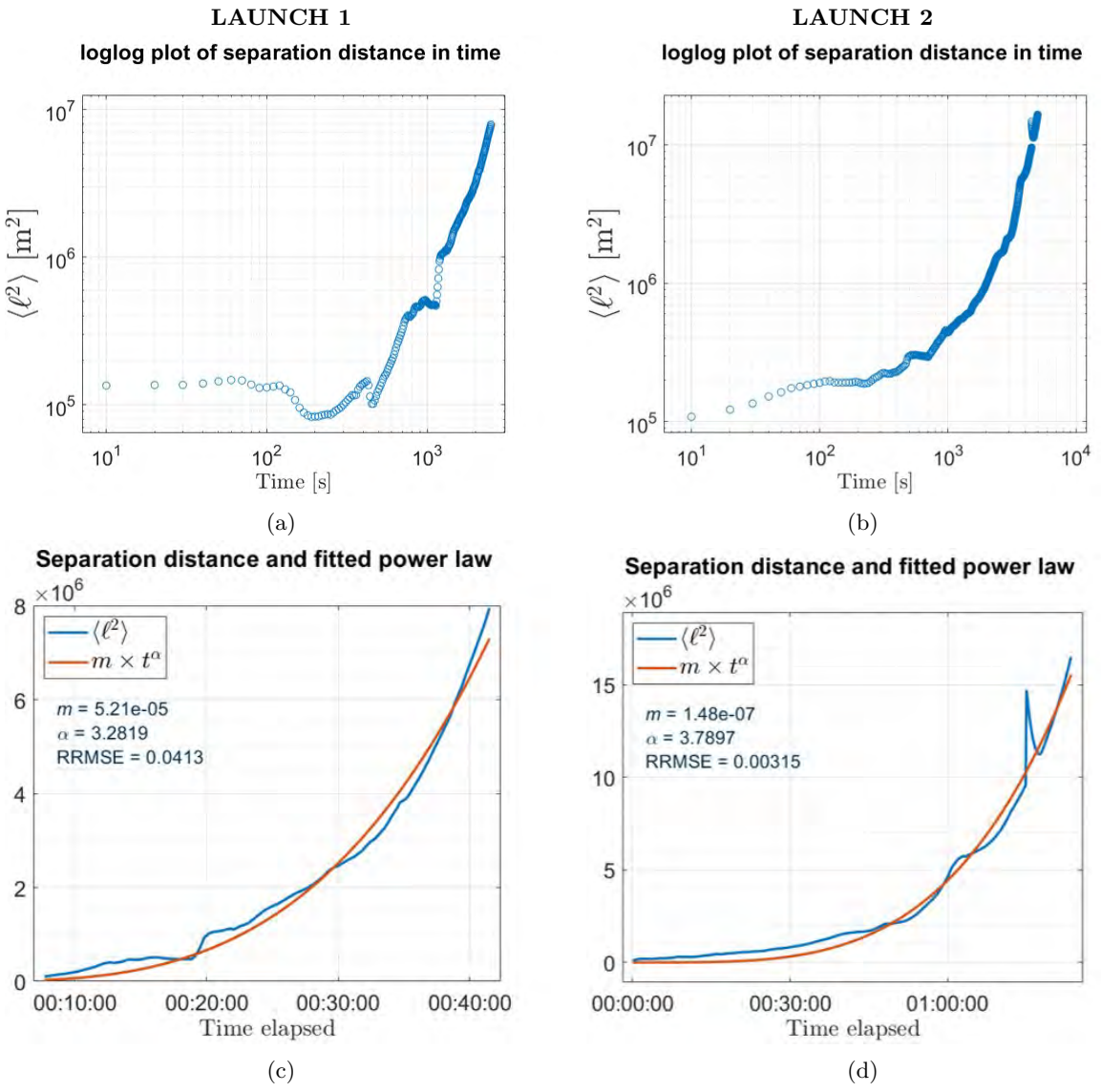

Figure 8: Mean relative distances and power law scaling. The left panels highlight the WESCON 2023 Chilbolton first launch, on July 5th, while the right panels show the second launch, on July 6th.

3 Relative dispersion analysis via distance - neighbor graph (Richardson, 1926)

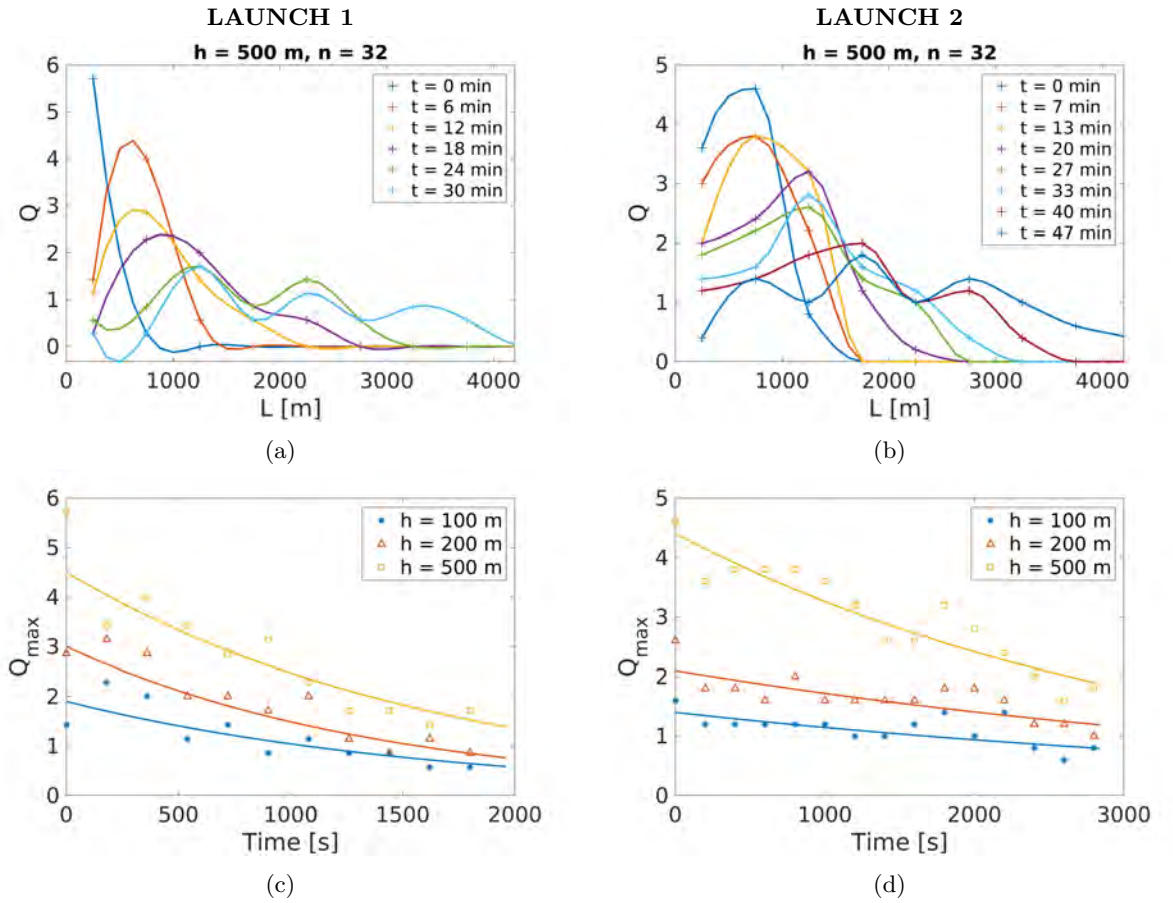

Figure 9: The distance-neighbor graph PDF computed from radiosonde position dataset. The left panels highlight the first launch, while the right panel shows the second launch. See below Table 1 for the scaling of exponential interpolations.

Table 1: Exponential scaling of number of neighbors inside neighborhood for different size of the neighborhood.

	Launch 1	Launch 2
H = 100 m	1.9 * exp(-0.0006 * t)	1.4 * exp(-0.0002 * t)
H = 200 m	3 * exp(-0.0007 * t)	2.1 * exp(-0.0002 * t)
H = 500 m	4.5 * exp(-0.0006 * t)	4.4 * exp(-0.0003 * t)

Table 2: Exponential scaling of relative distance (L_{max} or mean distance) within radiosonde cluster. L_{max} was computed for different values of neighborhood size, H.

	Launch 1	Launch 2
H = 100 m	463 * exp(0.0006 * t)	417 * exp(0.0005 * t)
H = 200 m	452 * exp(0.0006 * t)	444 * exp(0.0005 * t)
H = 500 m	501 * exp(0.0006 * t)	599 * exp(0.0004 * t)
Mean distance	450 * exp(0.0009 * t)	550 * exp(0.00045 * t)

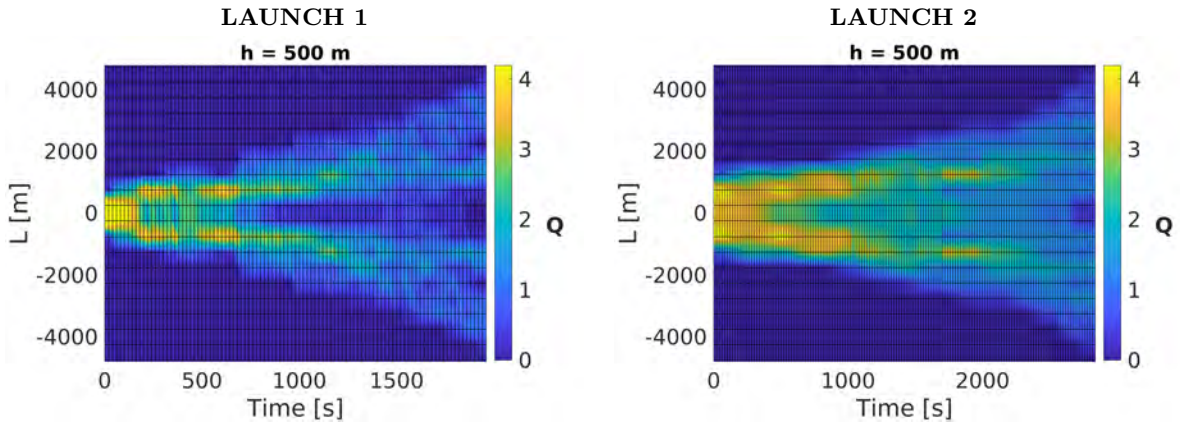

(a) (b)

Figure 10: A number of neighbors plotted over time and neighborhood bins. The left panel highlights the first launch, while the right panel shows the second launch.

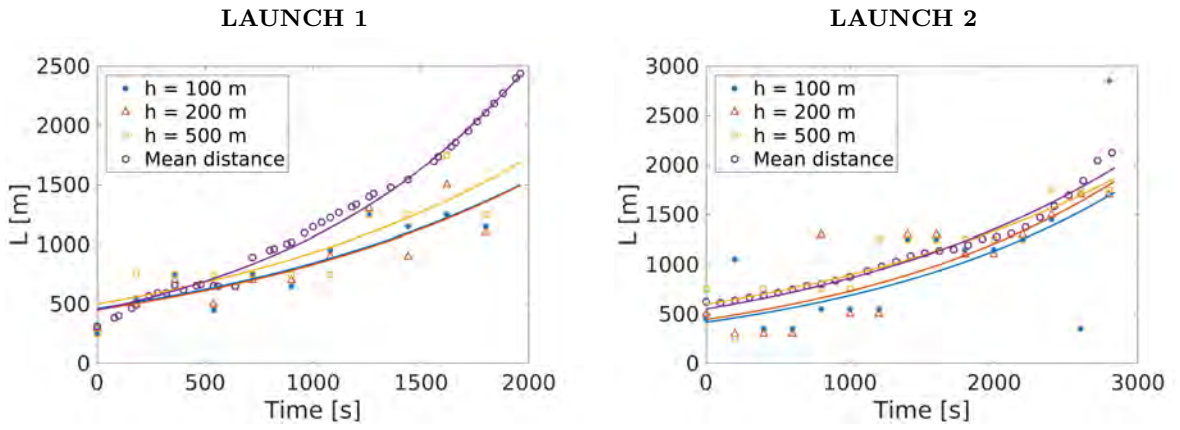

(a) (b)

Figure 11: Relative distance estimation comparison. The left panel highlights the first launch, while the right panel shows the second launch. See below Table 2 for the scaling of exponential interpolations.

4 Relative measurements and local turbulent characteristics from cluster dataset

Alpine boundary layer experiment. Valle d'Aosta, Nov 3, 2022.

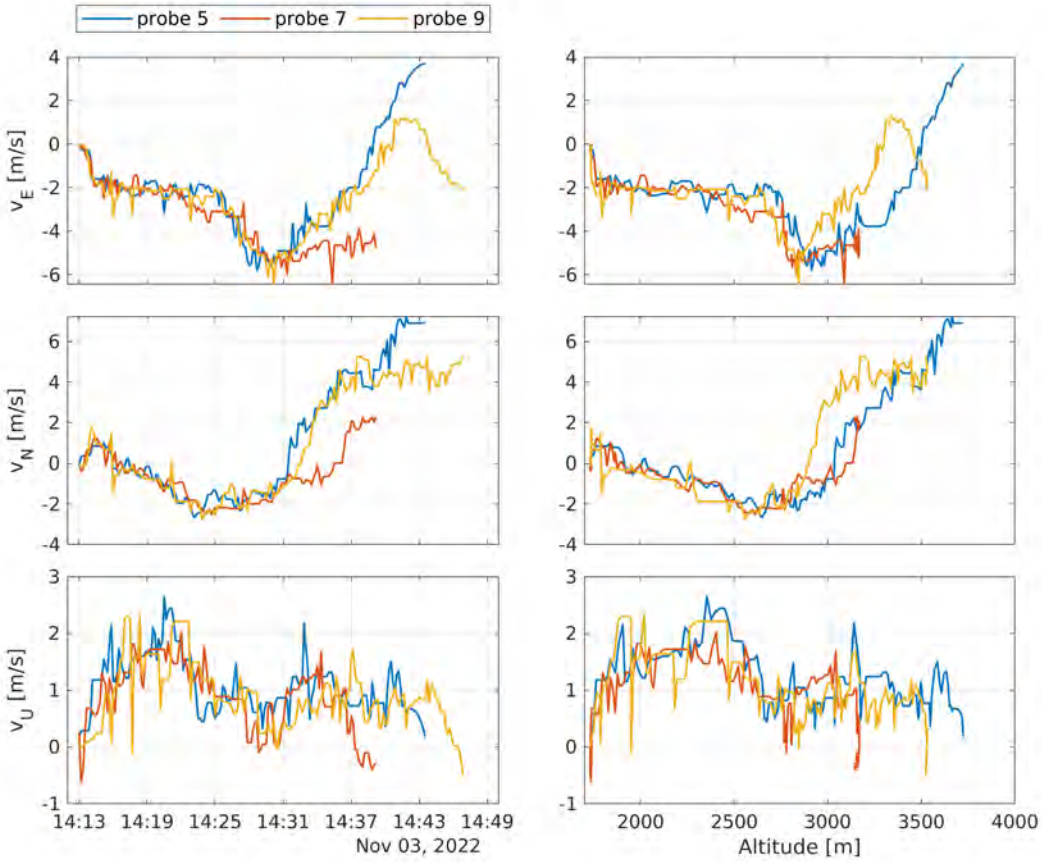

Figure 12: Measurements of East, North and Up velocity components from a subset of radiosondes.

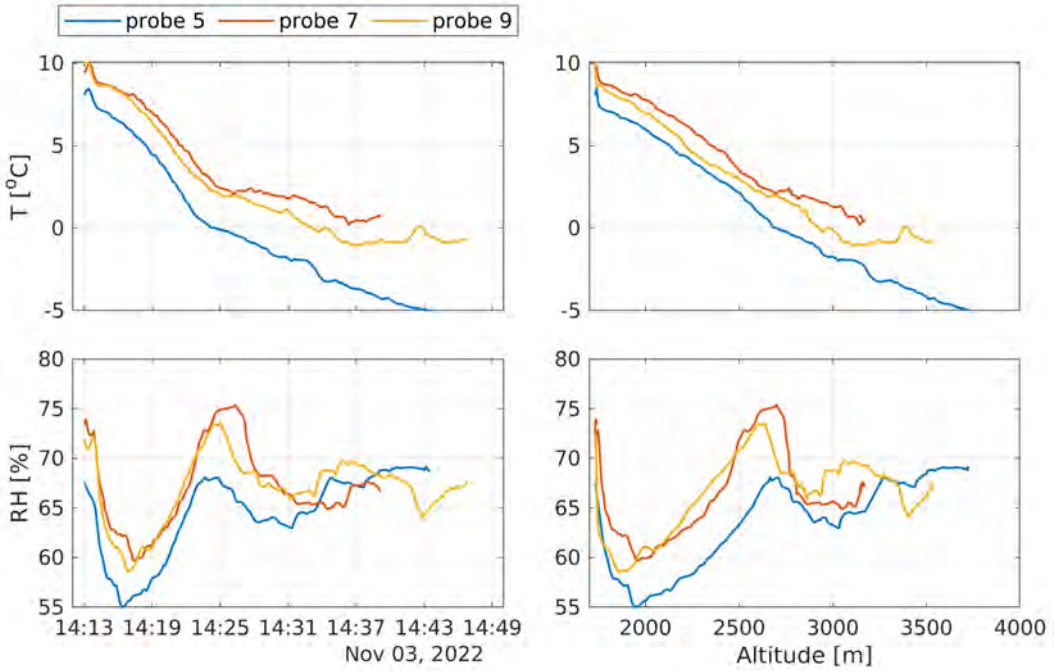

Figure 13: Measurements of temperature and humidity from a subset of radiosondes.

Alpine boundary layer experiment. Valle d'Aosta, Nov 3, 2022.

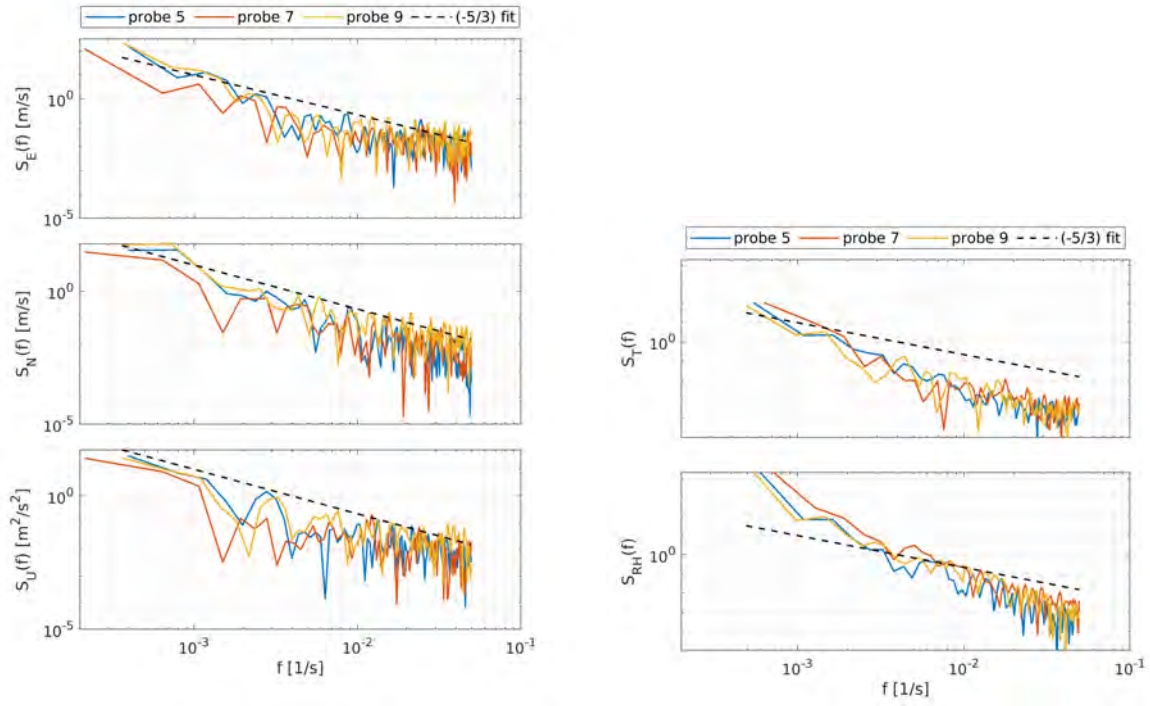

(a) (b)

Figure 14: Power spectral densities of velocity components, temperature and humidity from a subset of radiosondes. dt = 10s, dL = 30-35 meters for each dt timestep, dL/dt = 3-3.5 m/s.

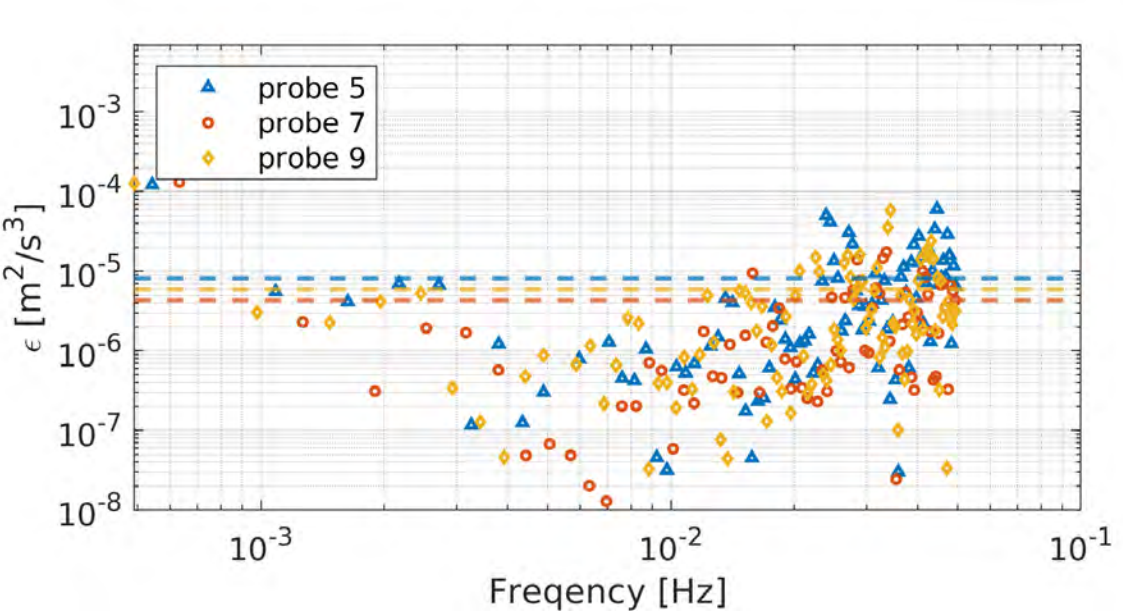

Figure 15: Mean energy dissipation rates computed from readings of subset of radiosondes (see Eq. 1 below). Estimated values (m2/s3): Probe 5 $= 1.4 * 10^{-5}$, Probe 7 $= 0.4 * 10^{-5}$, Probe 9 $= 0.8 * 10^{-5}$.

$$\overline{\varepsilon} = \frac{2\pi}{\overline{U}} \left(\frac{f^{5/3} S(f)}{\alpha} \right)^{3/2}$$

Figure 16: Equation 1

5 Lagrangian correlation analysis

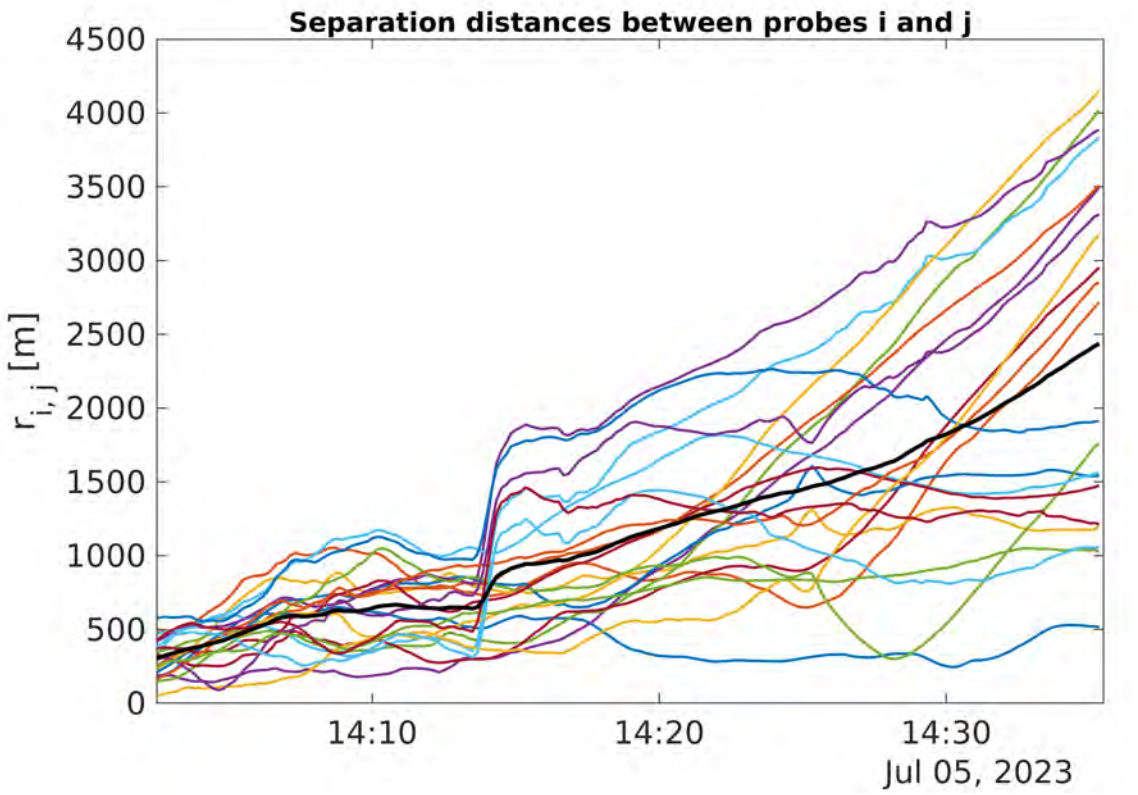

Figure 17: Separation distances over time between pair of radiosondes.

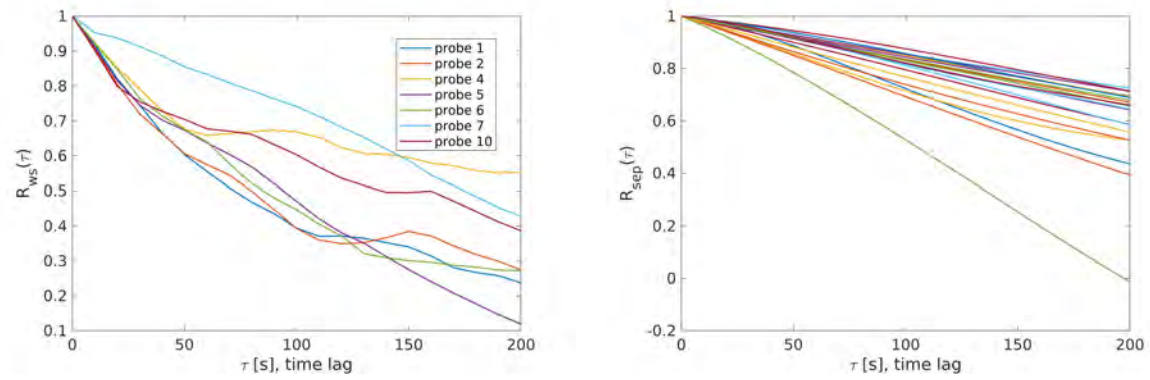

(a) (b)

Figure 18: Auto-correlations of horizontal wind speed and separation distance between pair of radiosondes.

6 From DNS simulation dataset

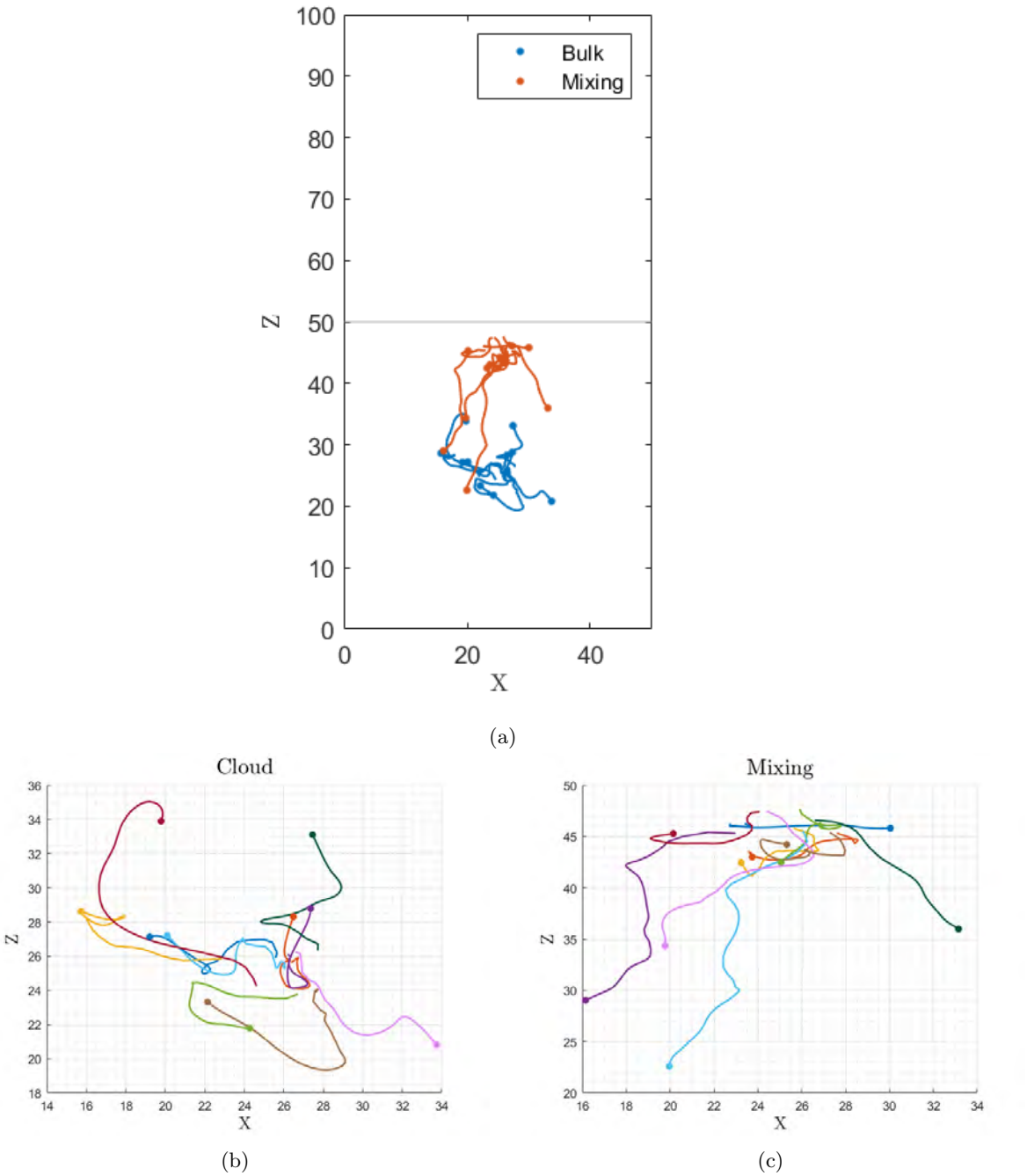

(a)

(b)

(c)

Figure 19: Trajectories of a small subset of water droplets within DNS simulation domain **???**. a) entire domain. b) inside the cloud, modeled as an homogeneous flow field. c) inside the shearless mixing region, modeling cloud-clear air boundary.

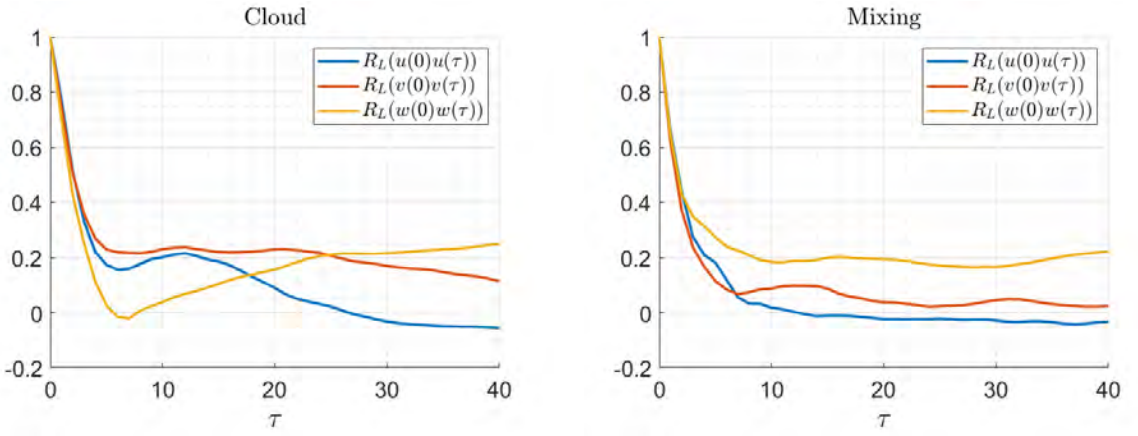

(a) (b)

Figure 20: Auto-correlations of horizontal wind speed and separation distance between pair of radiosondes.